INTERNATIONAL JOURNAL OF NOVEL RESEARCH AND DEVELOPMENT (IJNRD)
© 2026 IJNRD | Volume 11, Issue 3, March 2026 | ISSN: 2456-4184 | IJNRD.ORG

FORMULATION AND EVALUATION OF AMOXICILLIN LOADED FRUIT-BASED NANOFORMULATION

Ucheokoro Adaeze S.[1]*, Jackson Tenderwealth C.[2]

1. Department of Pharmaceutics and Pharmaceutical Technology, University of Port Harcourt, Port Harcourt 500004, Nigeria.
2. Department of Pharmaceutics and Pharmaceutical Technology, University of Uyo, Uyo, 520003, Nigeria.

Ucheokoro Adaeze S. is the Lead and the Corresponding Author

ABSTRACT

Background: Poor aqueous solubility and suboptimal dissolution limit the therapeutic performance of many oral antibiotics, including amoxicillin. Green nanotechnology offers a sustainable platform for enhancing drug delivery through plant-mediated nanoparticle synthesis.
Objective: This study aimed to formulate and evaluate amoxicillin-loaded fruit-based nano-formulations and assess their physicochemical characteristics and in-vitro dissolution performance relative to commercially available products.
Methods: Amoxicillin-loaded nanoparticles were synthesized via green reduction using *Carica papaya* and *Musa acuminata* fruit extracts with silver nitrate as precursor. The nano-formulations were characterized for particle size and stability using a Zeta sizer. In-vitro dissolution studies were performed using the USP paddle method in 0.1N HCl at 37 ± 1°C, and drug release was quantified spectrophotometrically. Results were compared with innovator and generic brands.
Results: The formulated nanoparticles were within the nanometric range, confirming successful nanoencapsulation. Optimized batches demonstrated enhanced dissolution profiles compared to reference products. Selected formulations achieved higher cumulative drug release within 60 minutes, indicating improved solubility and dispersion. The nanoscale size and increased surface area-to-volume ratio significantly contributed to the enhanced release kinetics. Stability assessment indicated acceptable formulation integrity under experimental conditions.
Conclusion: Fruit-mediated green synthesis successfully produced stable amoxicillin-loaded nano-formulations with improved in-vitro dissolution performance. These findings support the potential of sustainable nanotechnology approaches to enhance oral antibiotic bioavailability and therapeutic efficacy.

Keywords: Amoxicillin, Green synthesis, Silver nanoparticles, *In-vitro* dissolution, Nano-formulation.

INTRODUCTION

Amoxicillin, a semi-synthetic β-lactam antibiotic belonging to the aminopenicillin group, remains one of the most widely prescribed oral antibiotics globally for the treatment of bacterial infections such as respiratory tract infections, urinary tract infections, dental infections, otitis media, and Helicobacter pylori-associated peptic

ulcer disease.[1] It exerts its bactericidal effect by inhibiting bacterial cell wall synthesis through binding to penicillin-binding proteins, leading to cell lysis.[2] Despite its broad spectrum of activity against both Gram-positive and Gram-negative organisms, amoxicillin faces significant pharmaceutical and biopharmaceutical challenges that limit its therapeutic performance. As a Biopharmaceutics Classification System (BCS) Class III drug, it exhibits high solubility but low intestinal permeability, resulting in variable and incomplete oral absorption (bioavailability approximately 70–90%).[3] Its short biological half-life (1–1.5 hours) necessitates frequent dosing (every 8 hours), which often leads to poor patient compliance, fluctuating plasma concentrations, and sub-therapeutic levels at infection sites.[4] Additionally, amoxicillin is susceptible to acid-catalyzed degradation in the stomach and enzymatic inactivation by β-lactamases, further reducing its effectiveness and contributing to the growing problem of antimicrobial resistance.[5]

To overcome these limitations, advanced drug delivery systems, particularly nanoparticle-based formulations, have gained considerable attention in recent years. Nanoparticles (NPs) offer several advantages, including increased surface area for enhanced dissolution (following the Noyes-Whitney equation), protection of the drug from gastric degradation, improved permeability across biological membranes, controlled or sustained release, and the potential for targeted delivery to infection sites.[6] These features can significantly improve the dissolution profile, bioavailability, and therapeutic efficacy of amoxicillin while reducing dosing frequency and minimizing side effects[7].

Among the various nanoparticle platforms, fruit-based green synthesis has emerged as a sustainable, eco-friendly, and cost-effective approach. Fruit extracts from banana (*Musa acuminata*) and pawpaw (*Carica papaya*) are rich in bioactive phytochemicals such as ascorbic acid, polyphenols, flavonoids, carotenoids, and organic acids, which serve as natural reducing and capping agents for the synthesis of metal nanoparticles (e.g., silver nanoparticles, AgNPs).[8] This green method eliminates the use of toxic chemical reductants, minimizes environmental impact, and produces biocompatible nanoparticles with high stability and low cytotoxicity.[9] In resource-limited settings like Nigeria, where banana and pawpaw are abundantly available and inexpensive, fruit-based nanoparticles provide an attractive platform for local pharmaceutical innovation and reduction of dependence on imported synthetic excipients.[10]

The current study focuses on the formulation and evaluation of amoxicillin-loaded fruit-based nanoparticles using aqueous extracts of banana and pawpaw for the green synthesis of silver nanoparticles. Silver was chosen as the metal core due to its well-documented antimicrobial synergy with antibiotics, ability to disrupt bacterial membranes, and capacity to enhance drug penetration into biofilms.[11] The incorporation of amoxicillin into these fruit-mediated AgNPs is expected to improve its dissolution profile, stability, and antimicrobial activity through increased surface area, controlled release, and synergistic effects.[12]

This research is relevant because antimicrobial resistance is rising rapidly due to irrational use of antibiotics and poor formulation quality.[13] By developing a locally sourced nanoformulation, the study contributes to sustainable pharmaceutical development, supports local drug manufacturing, and addresses the need for improved antibiotic delivery systems in sub-Saharan Africa. The work evaluates key parameters such as morphology (SEM), thermal behaviour (DSC), functional groups (FTIR), and surface plasmon resonance (UV-Vis) to establish the impact of fruit type and drug loading on nanoparticle performance.

METHODS

Preparation of Deionized Water

A 300 mL of water was accurately measured, was transferred into an aspirator bottle and a water deionizer was connected to it. The tap of the aspirator bottle was turned on and the water was allowed to flow very slowly along the pipe of the deionizer after deionization and the deionized water was collected overtime in batches.

Fruits Extraction Procedure

The fruits of *Musa acuminata* (banana) and *Carica papaya* (pawpaw) were washed to remove dust and other debris. The water on the outer surface of the fruits was allowed to dry at room temperature. Fruit(s) peeling was done using knife, size reduction of a 50 g weight of each fruit was carried out using fruit juice extractor and then about 200 mL aqueous extracts from the fruits was obtained by filtration method using Whatman filter papers, funnels and beakers. The resultant extracts were set apart for further processing into nanoparticles.

Green Synthesis of $AgNO_3$ Nanoparticles

Different batches of nanoparticles comprising $AgNO_3$ and fruits extracts were prepared in accordance with the method of Jackson *et al.* (2019) with slight modification.[14]

Incorporation of the Model Drugs into the Nanoparticles

Table 1: Formula for Amoxicillin-Loaded Fruit-Based Nanoparticles Formulation

Ingredient	Amt./ Nanocapsule		Amt. / Nanocapsule		Amt. / Nanocapsule		Amt. / Nanocapsule		Amt. / Nanocapsule		Amt. / Nanocapsule	
Concentration	2.5% w/w		5.0% w/w		2.5% w/w		5.0% w/w		2.5% w/w		5.0% w/w	
Amoxicillin (mg)	75		75		125		125		250		250	
Silver nitrate ($AgNO_3$) (mg)	25		50		25		50		25		50	
Musa acuminate (M.a) (mg) *Carica papaya (C.p)* (mg)	*M.a*	*C.p*	*M.a*	*C.p*	*M.a*	*C.p*	*M.a*	*C.p*	*M.a*	*C.p*	*M.a*	*C.p*
	400	—	375	—	350	—	325	—	225	—	200	—
	—	400	—	375	—	350	—	325	—	225	—	200
Total weight of Amoxicillin nanocapsule (mg)	500		500		500		500		500		500	

Amoxicillin-Loaded Fruit-Based Nanoparticles

Amoxicillin-loaded fruit-based nanoparticles was formulated based on the formula in table 2.1. Petri-dishes were sterilized using a potable pressure steam autoclave (Model YX-24 LD) and were coded (labelled) accordingly. A 21.3 mL of fruit-based synthesized silver nanomaterial of 2.5 % w/w concentration was measured and was transferred to the well sterilized labelled petri-dish and 75 mg of amoxicillin pure drug was weighed and was incorporated into the nanomaterial in the petri-dish and was properly mixed with a magnetic stirrer. This procedure was carried out for different concentrations of silver nanoparticle (2.5 and 5.0 % w/w) and for different doses of amoxicillin pure drug samples (75 mg, 125 mg and 250 mg). Thereafter, the resultant / generated nanodrug (nano-formulation) colloid in different coded and capped petri-dishes were loaded into a

freeze-drying machine (freeze dryer) and left for 27 hours to enable the nanodrug colloid dry. Batches of dried nanodrug colloid was weighed, packed into labelled (coded) airtight containers in their respective batches. Individual amoxicillin nanodrug weight of 500 mg of various batches were obtained and subjected to further analyses (characterization).

Determination of surface Plasmon resonance of Nanodrugs using Ultraviolet–Visible Light Absorption Spectroscopy

A 0.5 mg quantity each of nanodrug samples was dissolved in 10 mL of distilled water, a 1 mL of the dissolved nanodrug was then placed in a spectralon plate of the UV/Visible instrument (PerkinElmer Lambdas 650-1050), fitted with a 150 mm center mount integrating sphere. The instrument background was then corrected and the nanodrug samples spectra and surface resonance were determined in scatter transmission and center mount mode.

Fourier Transform-Infrared Spectroscopy (FTIR)

About 10 mg quantity each of nanodrug samples was placed on a plate and sample pellets were formed. A smear was made and then sample alignment was determined (the blue lines were checked changed from red to green region). This was done and the nanodrug samples were placed for coding for peak determination, and the machine was set to pick the peaks, the peaks were selected and were properly labelled. FTIR analysis was carried out using Shimadzu FTIR, Model IR Affinity-1.

Morphological Studies of Nanodrug Samples

Scanning Electron Microscopy (SEM)

The scanning electron microscopy (SEM) was performed to examine the physical structure change of nanodrug samples using SEM model Phenom ProX, by phenomWorld Einhoven, Netherlands. Sample was placed on double adhesive which was on a sample stub, was coated by quorum technologies model Q150R, with 5nm of gold. Thereafter it was taken to the SEM machine chamber where it was viewed through NaVCaM for focusing and little adjustment. It was then transferred to SEM mode, focused and brightness contrasting was automatically adjusted, afterward the morphology of different magnification was determined and obtained.

Differential Scanning Calorimetry (DSC)

A differential scanning calorimetry studies were carried out using a Differential Scanning Calorimetry machine (Mettler Toledo, model DSC 822, Switzerland). The nanodrug sample was thoroughly dried, to avoid damaging the equipment and about 5mg of the sample was weighed and placed in an aluminum pan pierced lid in atmosphere of liquid nitrogen at the rate of 20 mL / minute within the temperature range of 27- 400 ^{o}C at 10 ^{o}C rise/minute at incremental rate to generate the thermograms for the nanodrug samples.

RESULTS AND DISCUSSION

Scanning Electron Microscopy (SEM) of Amoxicillin-loaded Fruit-Based Nanoparticles

Scanning Electron Micrograph of Amoxicillin-Loaded *Carica papaya*-Based Nanoparticles

Figures 1-3 below illustrate the scanning electron micrograph of amoxicillin-loaded *Carica papaya*-based nanoparticles.

Figure 1: Scanning Electron Micrograph of PA1a

Key: PA; P – Pawpaw (*Carica papaya*), A- Amoxicillin, 1 – 1st dose of amoxicillin pure sample (75 mg), a – 2.5 % w/v of $AgNO_3$ (1st concentration of silver nitrate).
PA is a sample batch of amoxicillin-loaded *Carica papaya*–based nanoparticle.

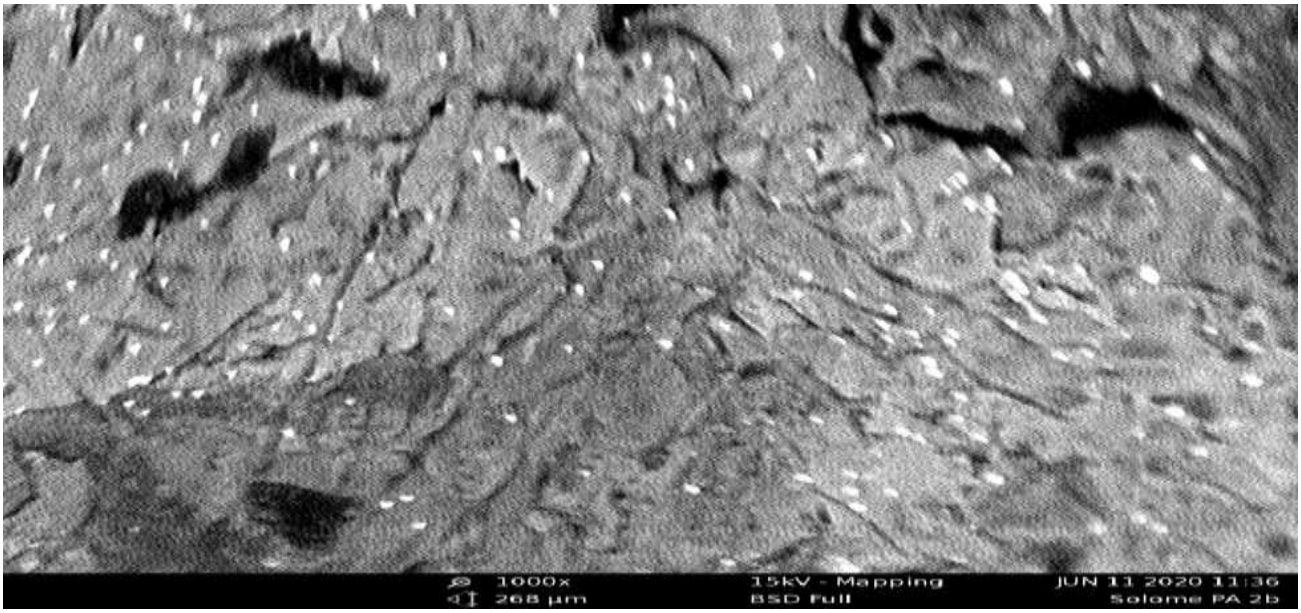

Figure 2: Scanning Electron Micrograph of PA2b

Key: PA; P – Pawpaw (*Carica papaya*), A- Amoxicillin, 2 – 2nd dose of amoxicillin pure sample (125 mg), b – 5.0 % w/v of $AgNO_3$ (2nd concentration of silver nitrate).
PA is a sample batch of amoxicillin-loaded *Carica papaya*–based nanoparticle.

Figure 3: Scanning Electron Micrograph of PA3a

Key: PA; P – Pawpaw (*Carica papaya*), A- Amoxicillin, 3 – 3rd dose of amoxicillin pure sample (250 mg), a – 2.5 % w/v of $AgNO_3$ (1st concentration of silver nitrate).
PA is a sample batch of amoxicillin-loaded *Carica papaya*–based nanoparticle.

Scanning Electron Micrograph of Amoxicillin-Loaded *Musa acuminata*-Based Nanoparticles

Figures 4-6 below illustrate the scanning electron micrograph of amoxicillin-loaded *Musa acuminata*-based nanoparticles.

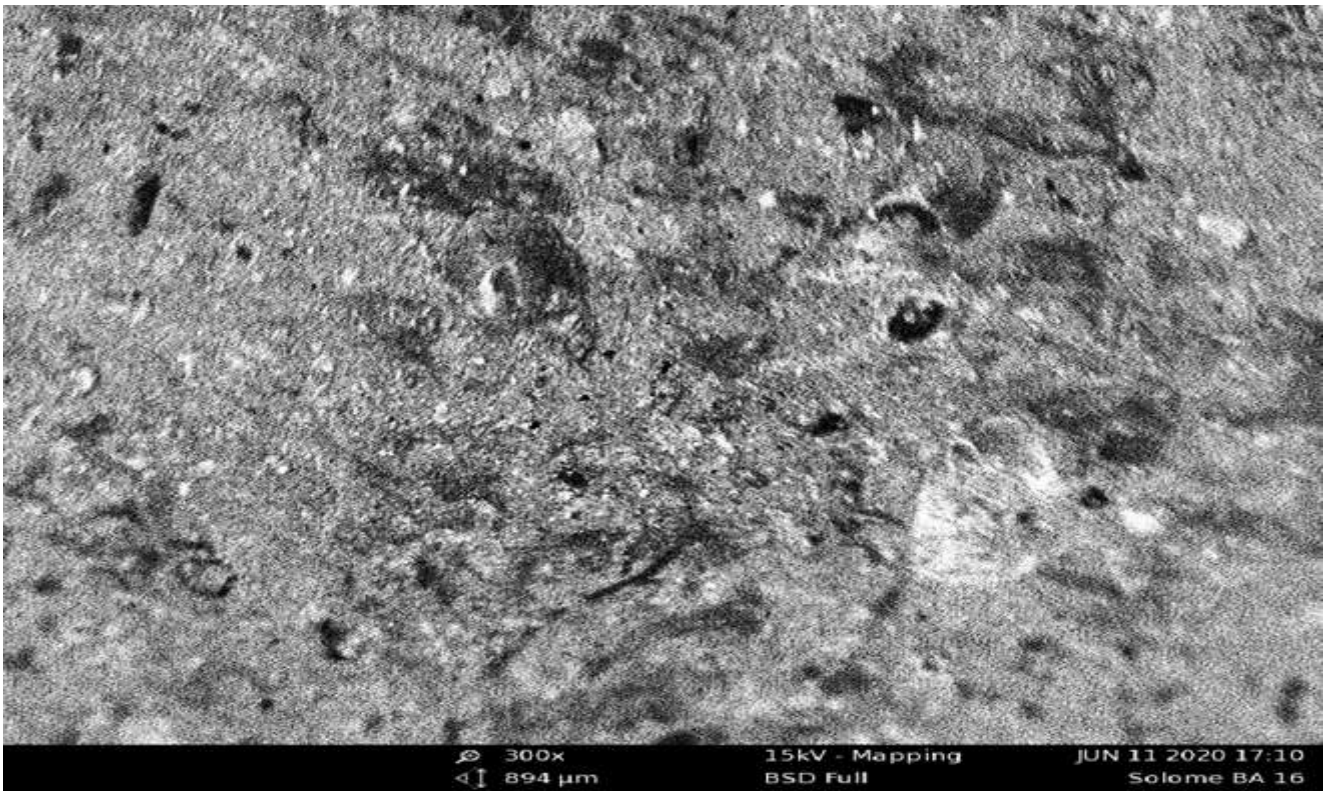

Figure 4: Scanning Electron Micrograph of BA1b

Key: BA; B - Banana (*Musa acuminata*), A- Amoxicillin, 1 – 1st dose of amoxicillin pure sample (75 mg), b – 5.0 % w/v of $AgNO_3$ (2nd concentration of silver nitrate).
BA is a sample batch of amoxicillin-loaded *Musa acuminata*–based nanoparticle.

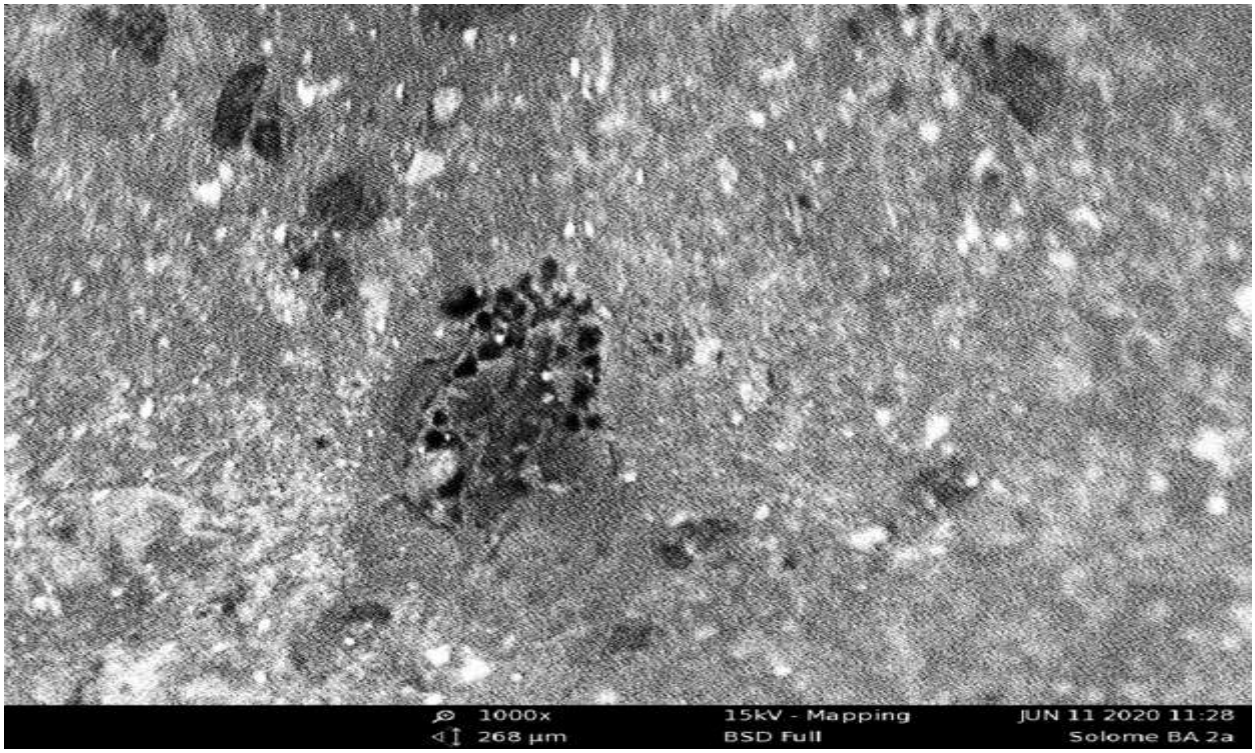

Figure 5: Scanning Electron Micrograph of BA2a

Key: BA; B - Banana (*Musa acuminata*), A- Amoxicillin, 2 – 2nd dose of amoxicillin pure sample (125 mg), a – 2.5 % w/v of $AgNO_3$ (1st concentration of silver nitrate).
BA is a sample batch of amoxicillin-loaded *Musa acuminata*–based nanoparticle.

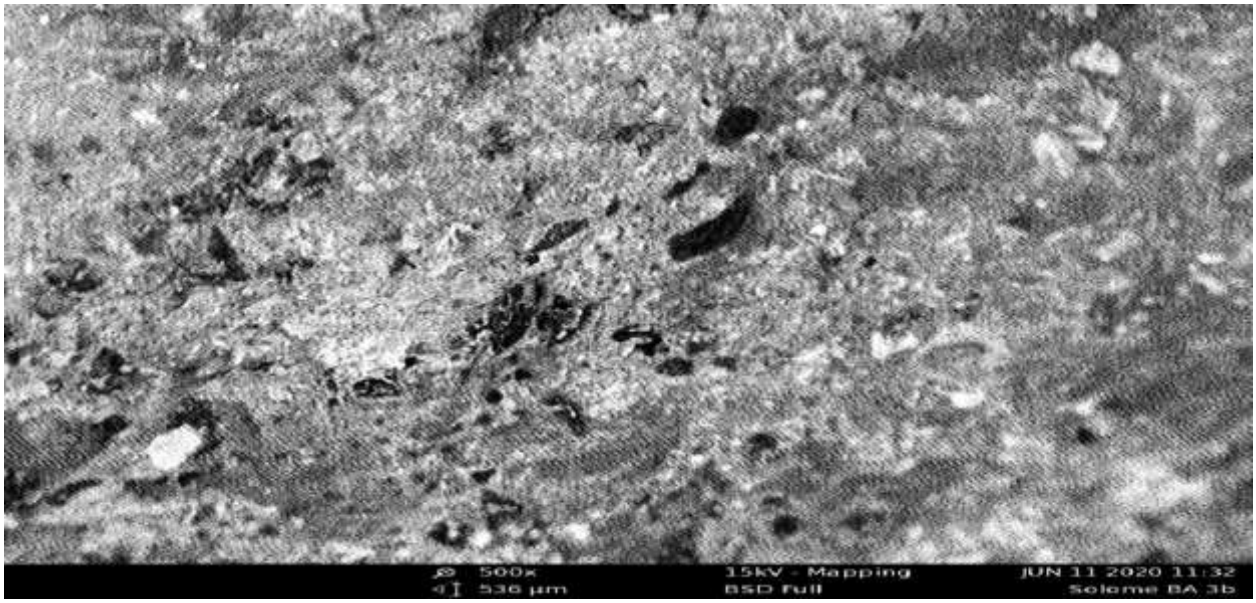

Figure 6: Scanning Electron Micrograph of BA3b

Key: BA; B - Banana (*Musa acuminata*), A- Amoxicillin, 3 – 3rd dose of amoxicillin pure sample (250 mg), b – 5.0 % w/v of $AgNO_3$ (2nd concentration of silver nitrate).
BA is a sample batch of amoxicillin-loaded *Musa acuminata*–based nanoparticle.

Scanning Electron Micrograph of Amoxicillin Pure Sample

Figure 7 below illustrates the scanning electron micrograph of amoxicillin pure sample

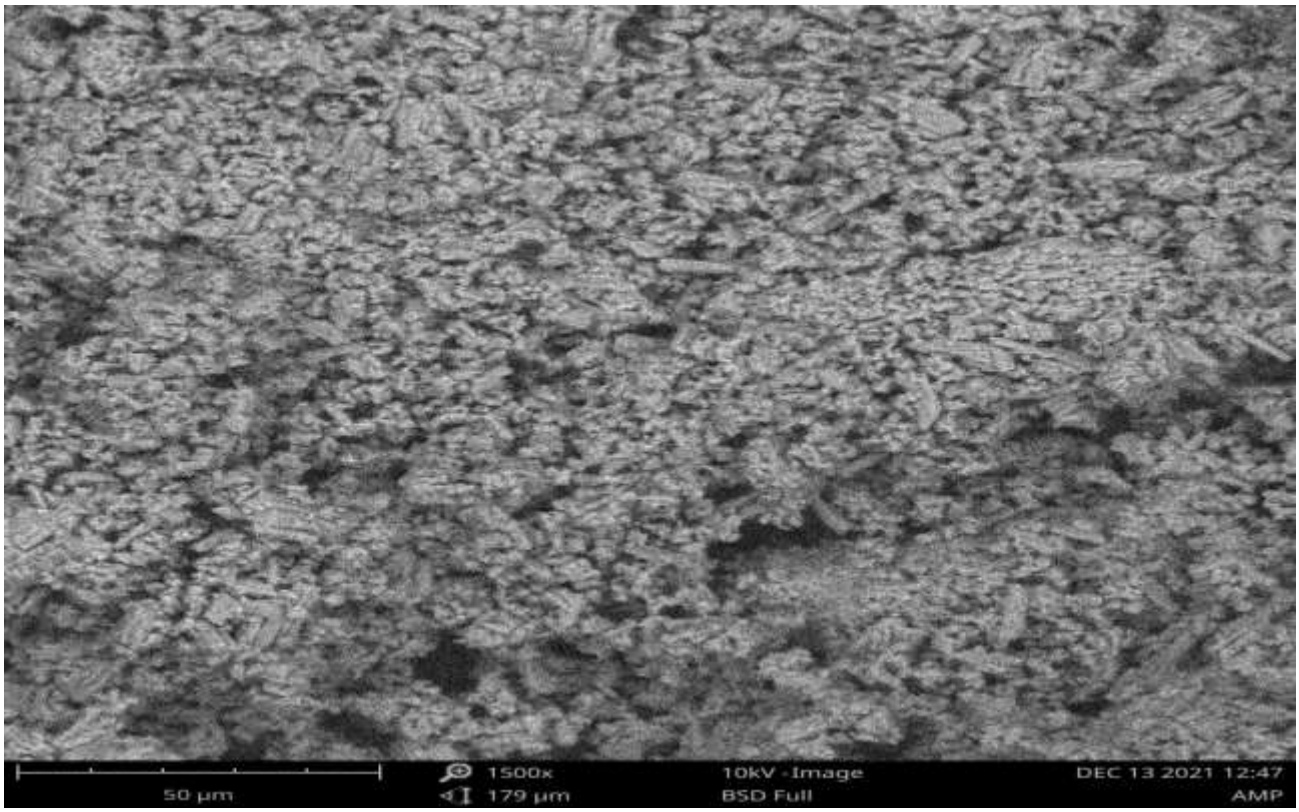

Figure 7: Scanning Electron Micrograph of Amoxicillin Pure Sample

The micrographs (SEM) of amoxicillin loaded fruit-based nanoparticles and pure sample are respectively shown in figures 1 to 7 and showed that synthesized nanoparticles appeared as spherical colloidal nanoparticles.[15] The samples morphology showed that the nanoparticles had a certain degree of surface roughness. The ridges and surface roughness enhance and cause an increase in contact surface, contributing to more (increased) number of active sites on the colloidal surface of the nanoparticles which therefore, causes an increase in the surface area available for enzyme immobilization (nanoparticles mechanism of action).[16]

Thermal Analysis (Differential Scanning Calorimetry, DSC) of Amoxicillin-Loaded Fruit-Based Nanoparticles

Thermogram of Amoxicillin-Loaded *Carica papaya* and *Musa acuminata*-Based Nanoparticles, Respectively

Figures 8-10 illustrate the thermograms of amoxicillin-loaded *Carica papaya* and *Musa*

acuminata-based nanoparticles, respectively.

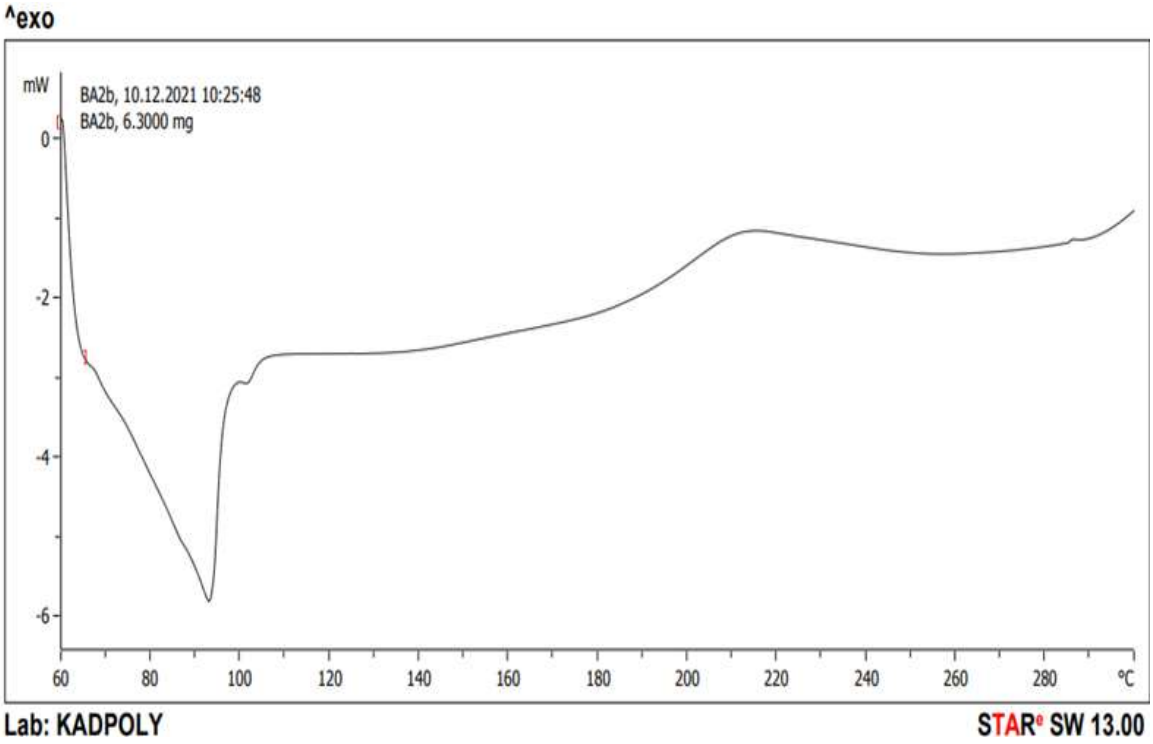

Figure 8: DSC Thermogram of BA2b

Key: BA; B – Banana (*Musa acuminata*), A - Amoxicillin, 2 – 2nd dose of amoxicillin pure sample (125 mg), b – 5.0 % w/v of $AgNO_3$ (2^{nd} concentration of silver nitrate).
BA is a sample batch of amoxicillin-loaded *Musa acuminata*–based nanoparticle.

BA2b showed a melting point of 94 ^oC

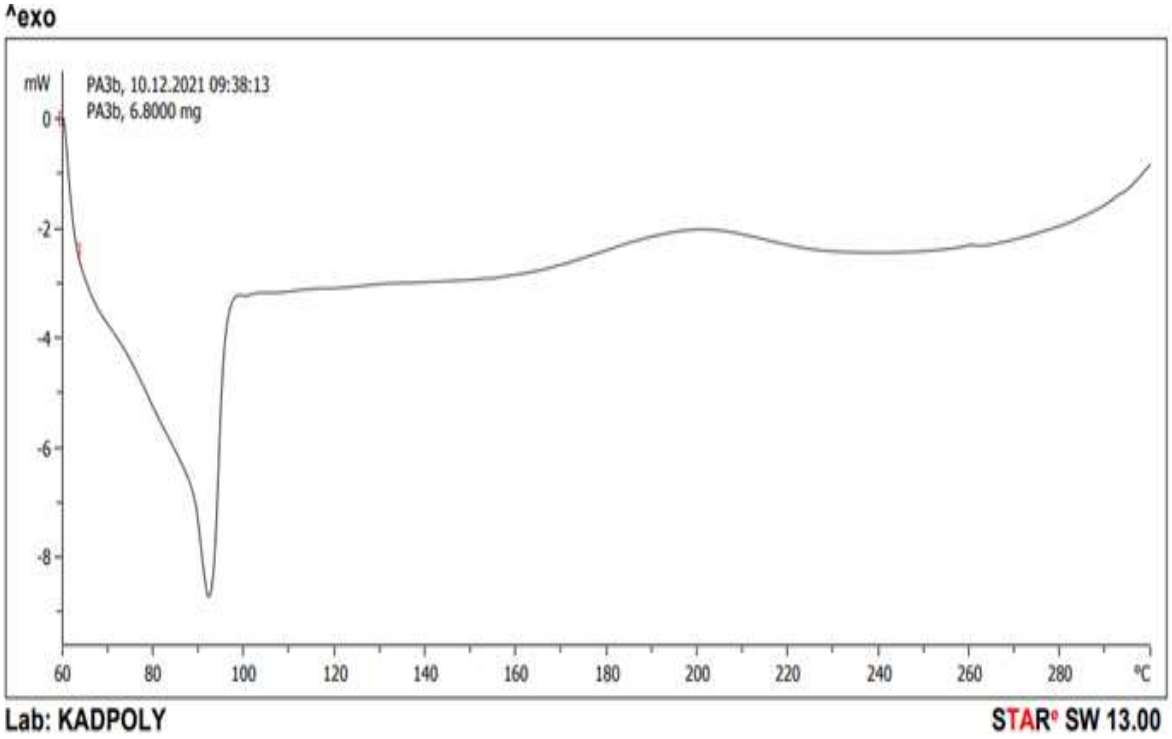

Figure 9: DSC Thermogram of PA3b

Key: PA; P – Pawpaw (*Carica papaya*), A - Amoxicillin, 3 – 3rd dose of amoxicillin pure sample (250 mg), b – 5.0 % w/v of $AgNO_3$ (2nd concentration of silver nitrate).
PA is a sample batch of amoxicillin-loaded *Carica papaya*–based nanoparticle.

PA3b showed a melting point of 92 ^oC

Thermogram of Amoxicillin Pure Sample

Figure 10 illustrates the thermogram of amoxicillin pure sample.

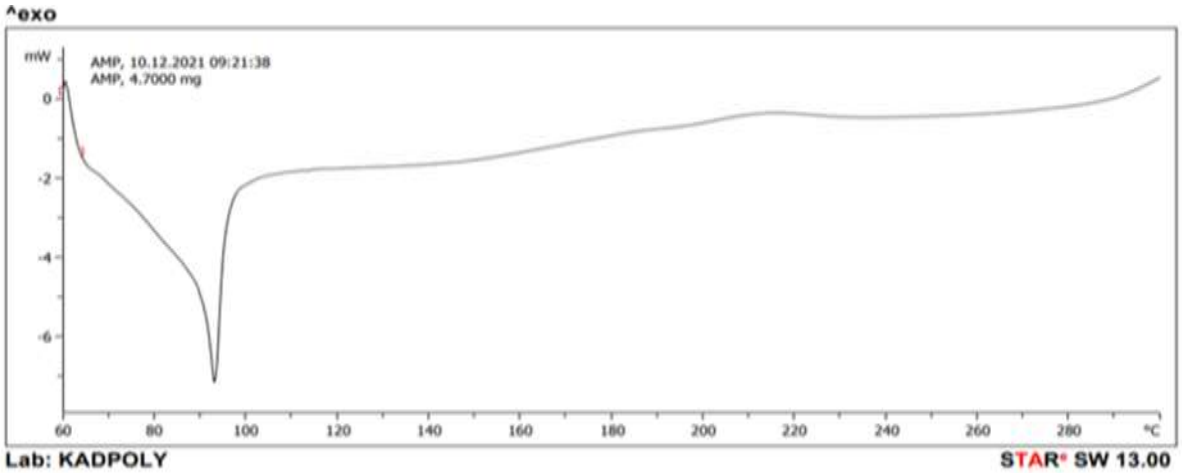

Figure 10: DSC Thermogram of Amoxicillin Pure Sample

Amoxicillin pure sample showed a melting point of 92 ^oC.

Figures 8 to 10 illustrate the thermograms of amoxicillin loaded fruit-based nanoparticles and showed endothermic peak range of 94 ºC and 92 ºC, respectively, while the amoxicillin pure sample displayed in figure 10 showed an endothermic peak of 92 ºC. These endothermic peak ranges could be as a result of aqueous liquid loss during freeze drying which occurred within 6 min-6.75 min and exothermic peak of above 210 was obtained within 4.5 min-4.54 min which may be as a result of cross or recrystallization reaction and thermal decomposition of silver nanoparticles.[17-19]

Fourier Transform InfraRed Spectroscopy (FTIR) of Amoxicillin and Metronidazole-Loaded Fruit-Based Nanoparticles

FTIR Spectroscopy of *Carica papaya*-Based Amoxicillin Nanoparticles

Figures 11-13 showed the FTIR spectroscopy of *Carica papaya*-based amoxicillin nanoparticles.

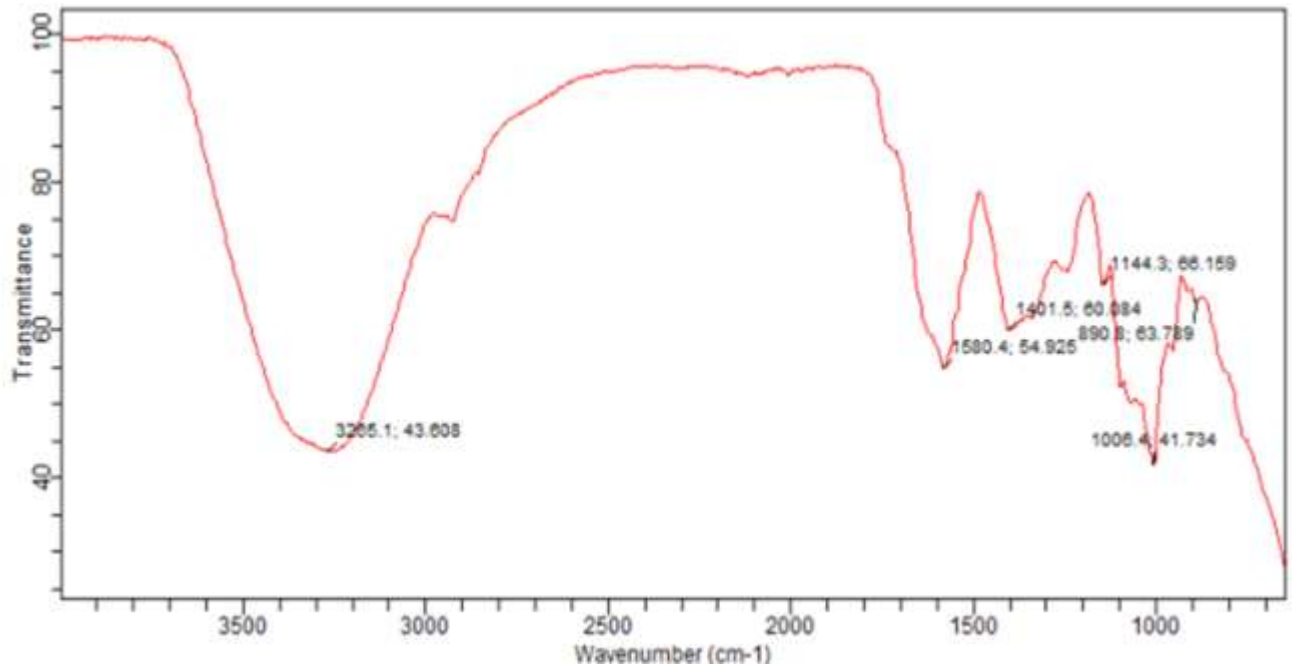

Figure 11: FTIR of PA1a

Key: PA; P – Pawpaw (*Carica papaya*), A - Amoxicillin, 1–1st dose of amoxicillin pure sample (75 mg), a – 2.5 % w/v of $AgNO_3$ (1st concentration of silver nitrate).

PA is a sample batch of amoxicillin-loaded *Carica papaya*–based nanoparticle.

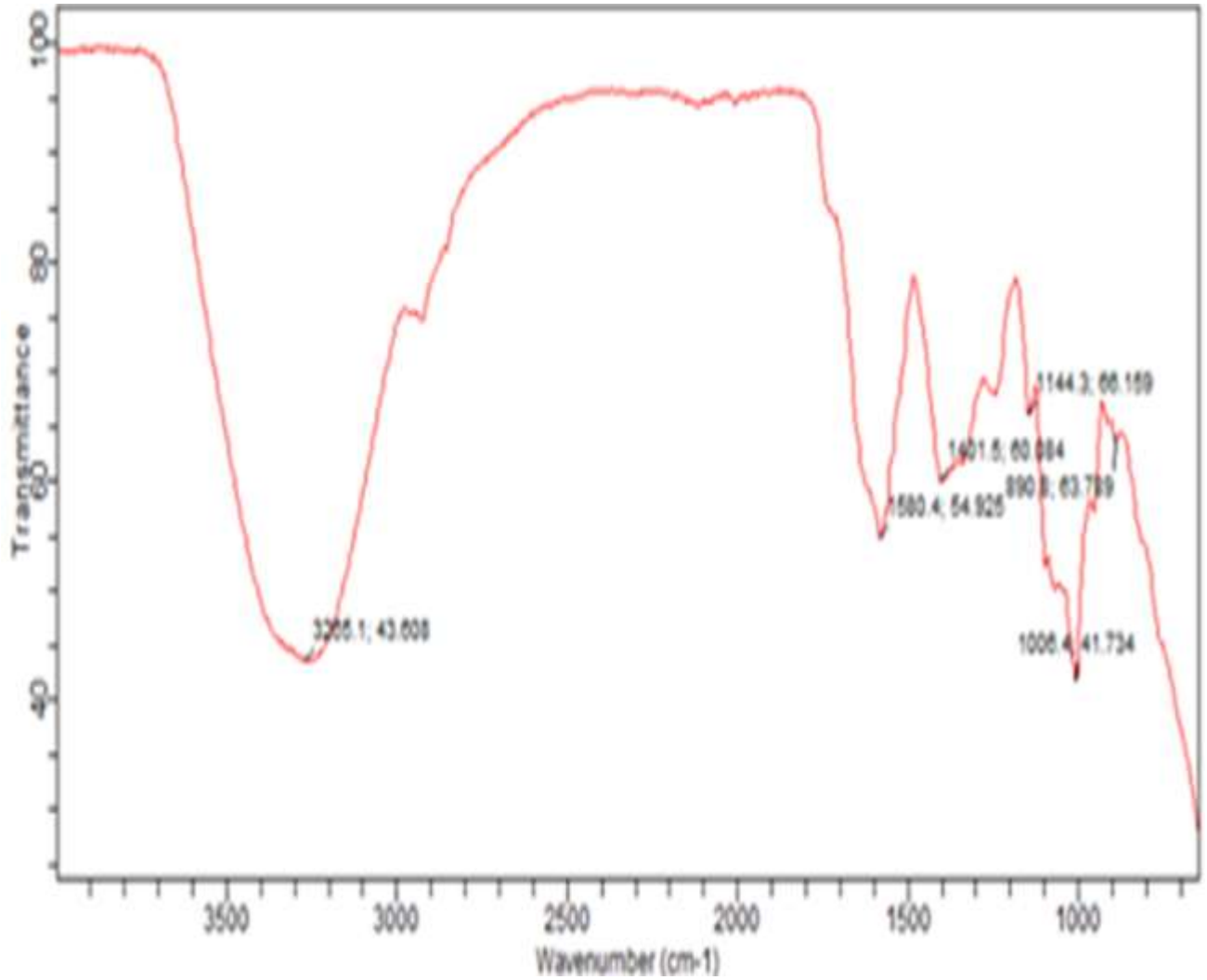

Figure 12: FTIR of PA2b

Key: PA; P – Pawpaw (*Carica papaya*), A - Amoxicillin, 1–1st dose of amoxicillin pure sample (75 mg), a – 2.5 % w/v of $AgNO_3$ (1^{st} concentration of silver nitrate).
PA is a sample batch of amoxicillin-loaded *Carica papaya*–based nanoparticle.

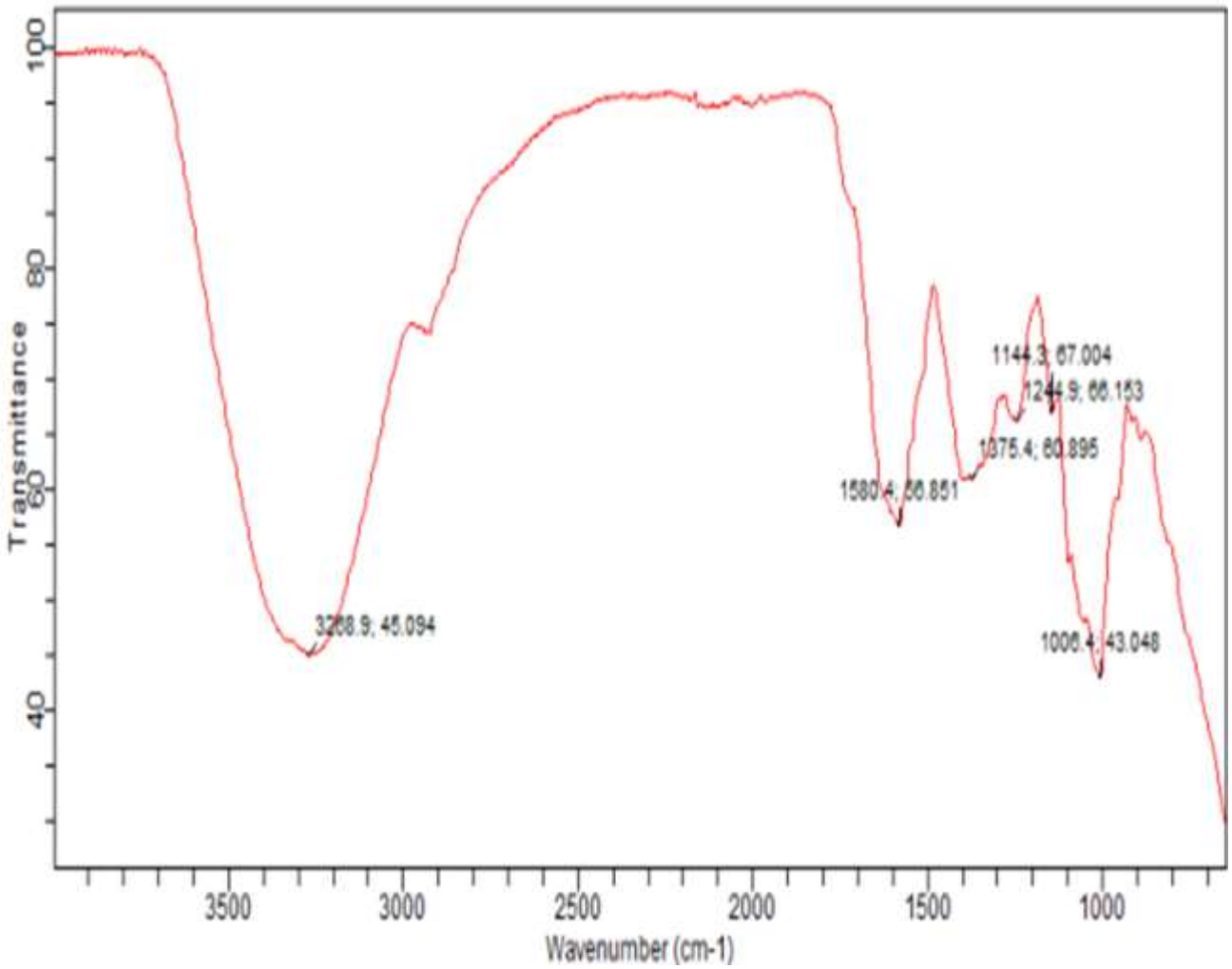

Figure 13: FTIR of PA3a

Key: PA; P – Pawpaw (*Carica papaya*), A - Amoxicillin, 3–3rd dose of amoxicillin pure sample (250 mg), a – 2.5 % w/v of $AgNO_3$ (1st concentration of silver nitrate).
PA is a sample batch of amoxicillin-loaded *Carica papaya*–based nanoparticle.

FTIR Spectroscopy of *Musa acuminata*-Based Amoxicillin Nanoparticles

Figures 14-17 illustrate the FTIR spectroscopy of *Musa acuminata*-based amoxicillin nanoparticles.

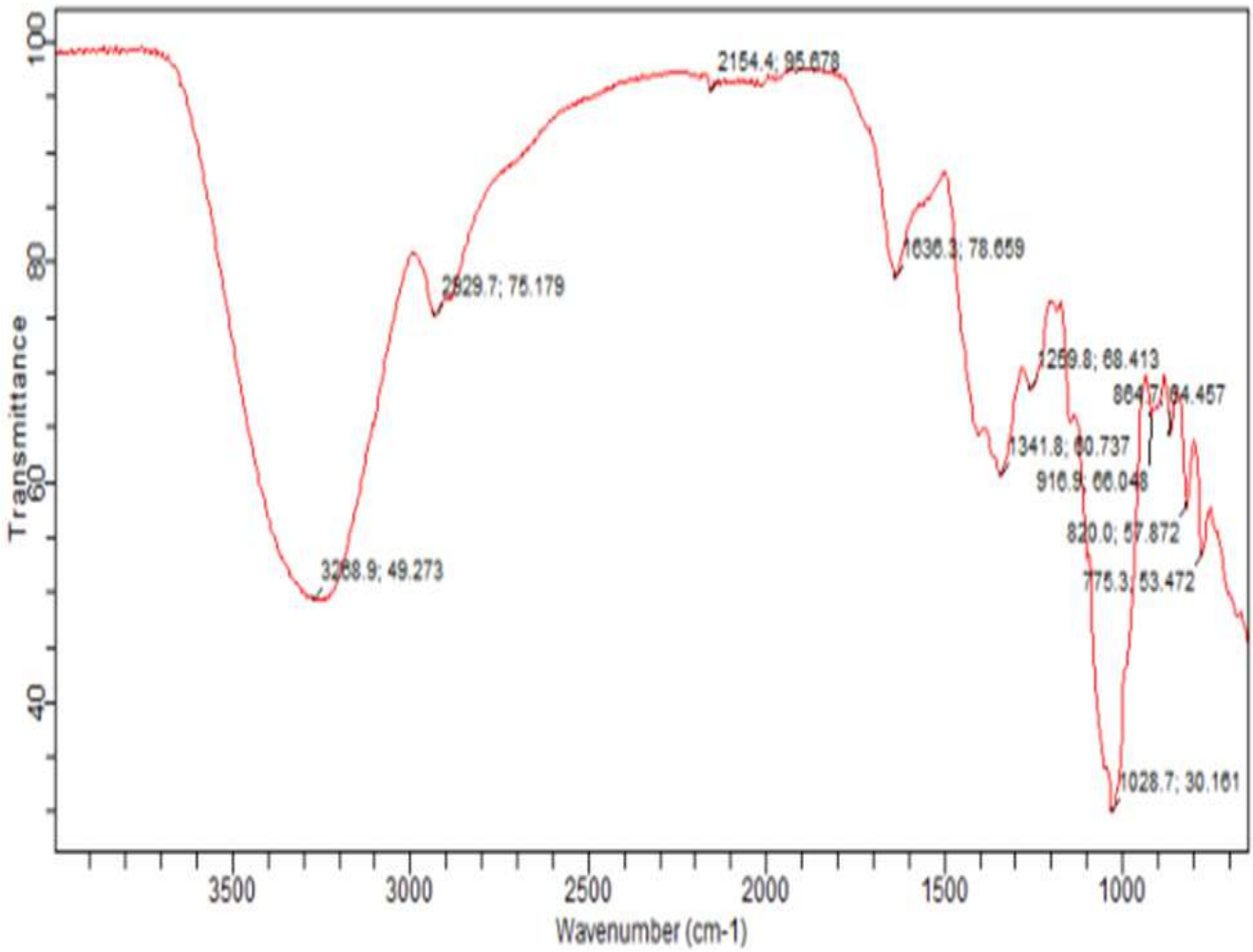

Figure 14: FTIR of BA1b

Key: BA; B – Banana (*Musa acuminata*), A - Amoxicillin, 1–1st dose of amoxicillin pure sample (75 mg), b – 5.0 % w/v of $AgNO_3$ (2nd concentration of silver nitrate).
BA is a sample batch of amoxicillin-loaded *Musa acuminata*–based nanoparticle.

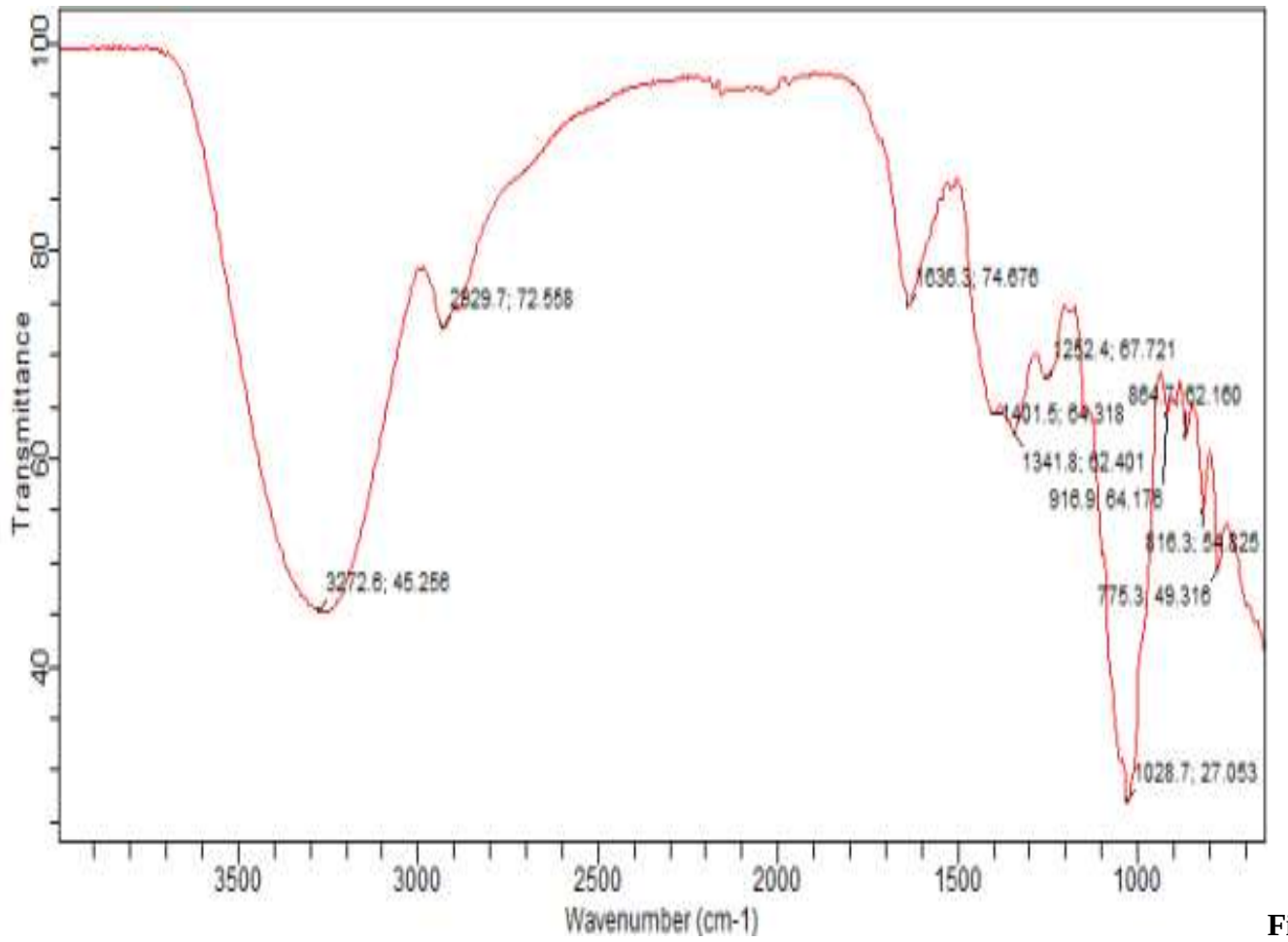

Figure 15: FTIR of BA2a

Key: BA; B – Banana (*Musa acuminata*), A - Amoxicillin, 2–2nd dose of metronidazole pure sample (100 mg), a – 2.5 % w/v of $AgNO_3$ (1st concentration of silver nitrate).
BA is a sample batch of amoxicillin-loaded *Musa acuminata*–based nanoparticle.

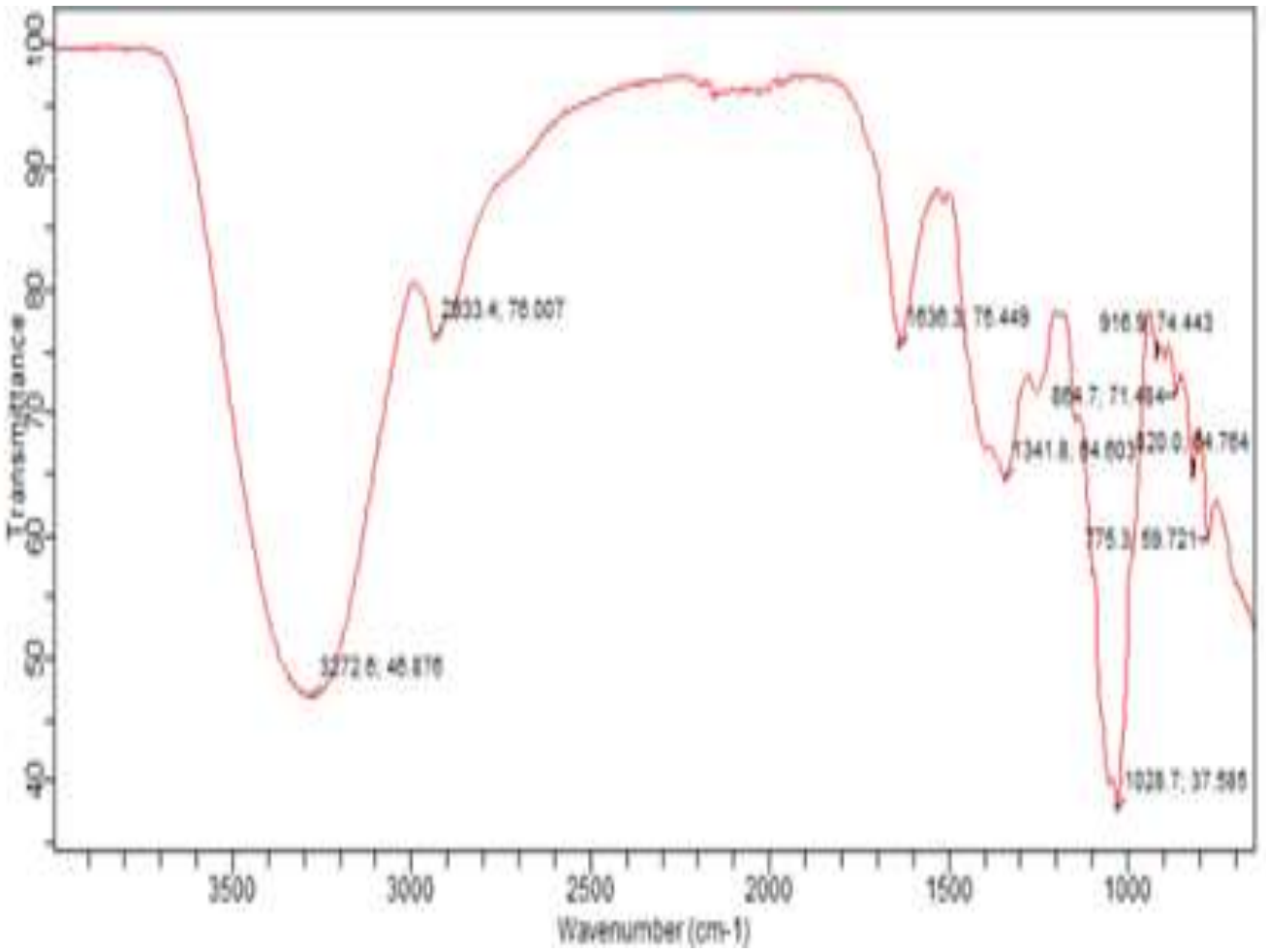

Figure 16: FTIR of BA3b

Key: BA; B – Banana (*Musa acuminata*), A - Amoxicillin, 3–3rd dose of amoxicillin pure sample (100 mg), b – 5.0 % w/v of $AgNO_3$ (2nd concentration of silver nitrate).
BA is a sample batch of amoxicillin-loaded *Musa acuminata*–based nanoparticle.

FTIR Spectroscopy of Amoxicillin Pure Sample

Figure 17 illustrates the FTIR spectroscopy of amoxicillin pure sample.

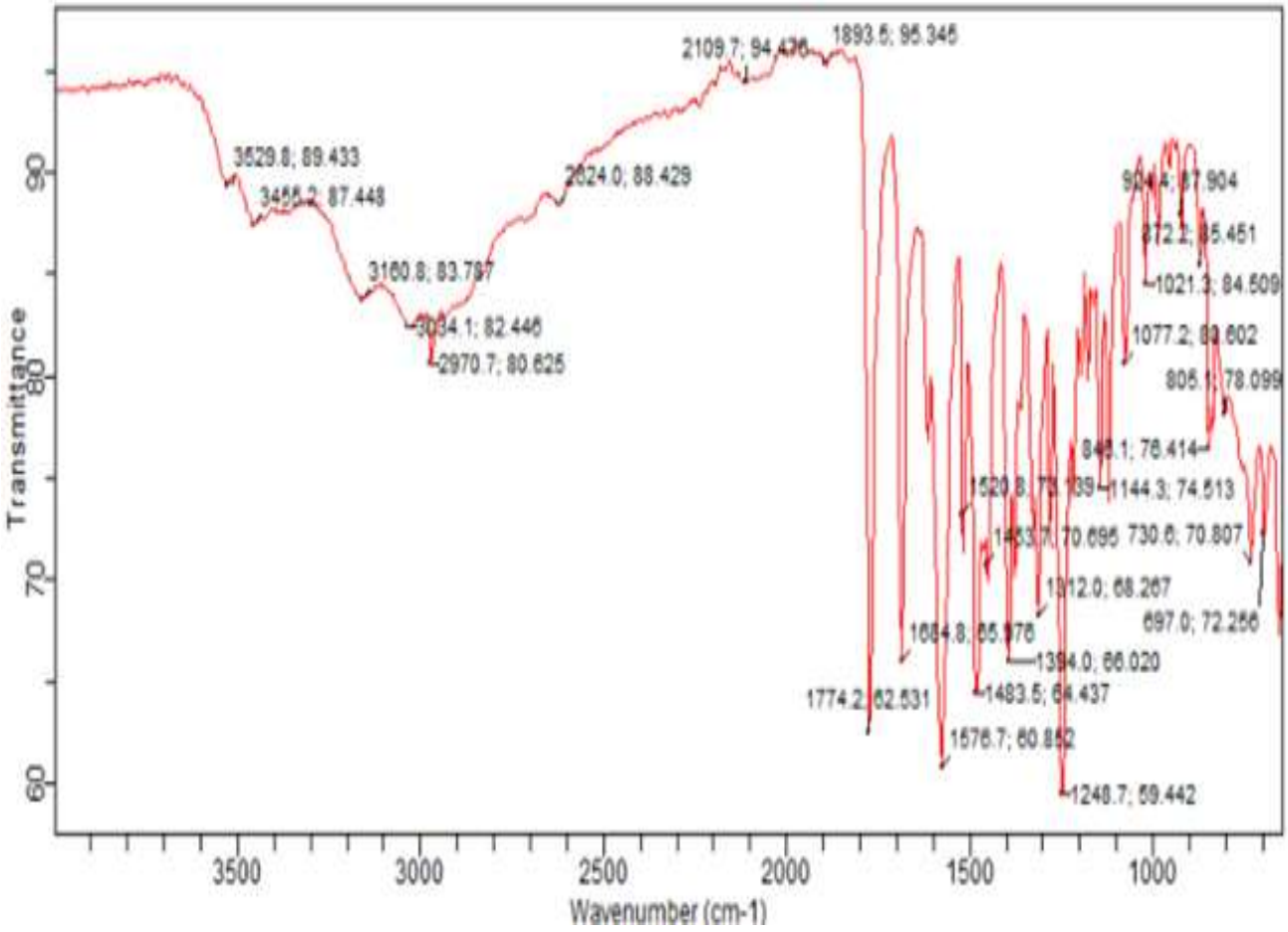

Figure 17: FTIR of Amoxicillin Pure Sample

Fourier Transmission Infrared Spectroscopy (FTIR) of amoxicillin pure samples in figure 17 showed broad band peak at 3529.8 cm^{-1}. While, in figures 14-16 amoxicillin-loaded fruit-based nanoparticles showed broad band peak at ranges of 3268.9-3272.6 cm^{-1} which is relative to the hydroxyl (-OH) group of phenol molecules. Additionally, these fruit-based nanoparticles also showed a broad band range of about 1535 which reportedly was proven to correspond to the carbonyl groups in amide linkages or stretching vibration of C=O group neighbour to C=C double bonds. There are other peaks which are between 675 cm^{-1} – 1018 cm^{-1}, relative to C=OH stretching of secondary alcohols, C-H aromatic compound and C-Cl alkyl halides, respectively. **[20,21]**

Ultraviolet–Visible Light Absorption Spectroscopy of Amoxicillin-Loaded Fruit-Based Nanoparticles

Ultraviolet–Visible Light Absorption Spectroscopy of *Carica papaya*-Based Amoxicillin Nanoparticles

Figures 18-20 illustrate the Ultraviolet–Visible Light Absorption Spectroscopy of *Carica papaya*- based amoxicillin nanoparticles.

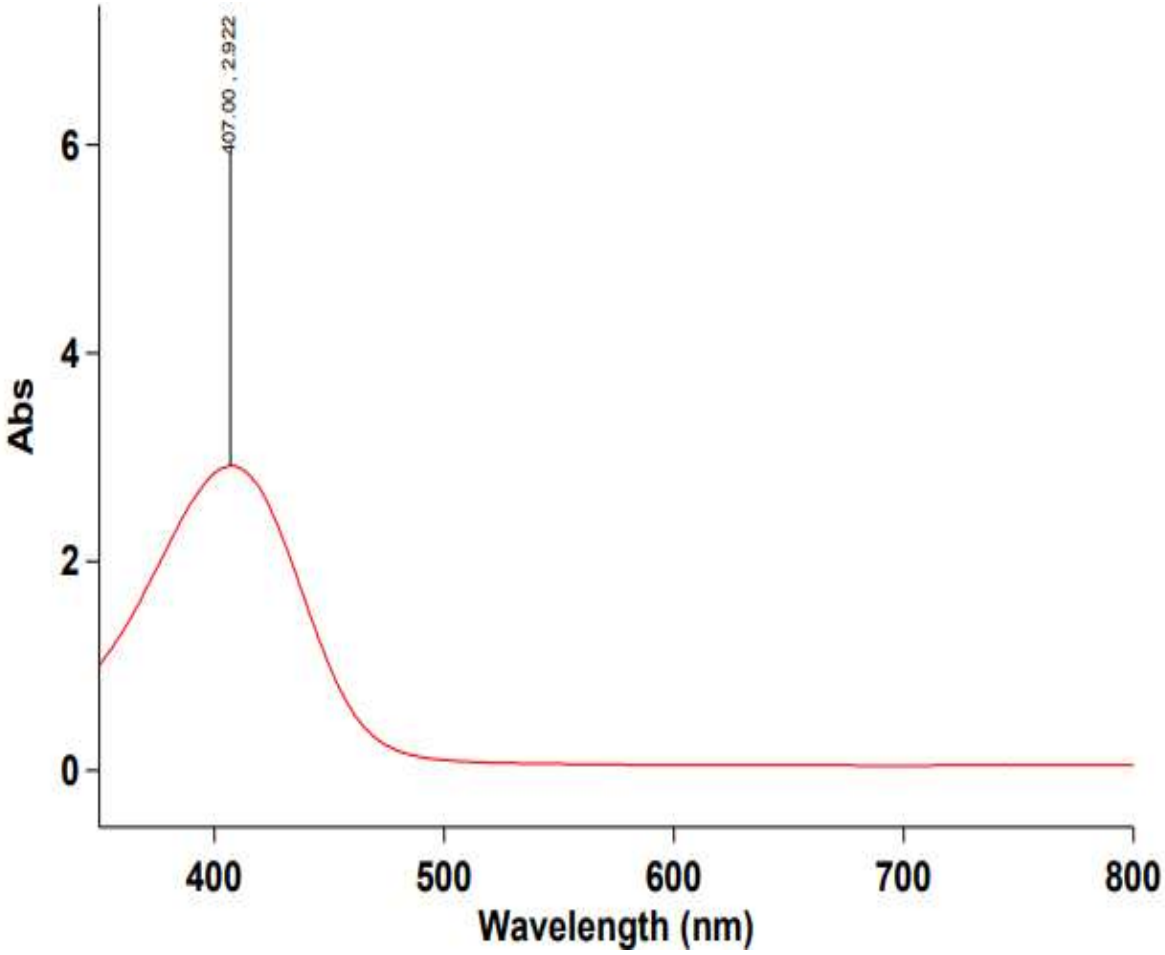

Figure 18: Ultraviolet–Visible Light Absorption Spectroscopy of PA1a

PA1a showed a UV peak of 407 nm wavelength

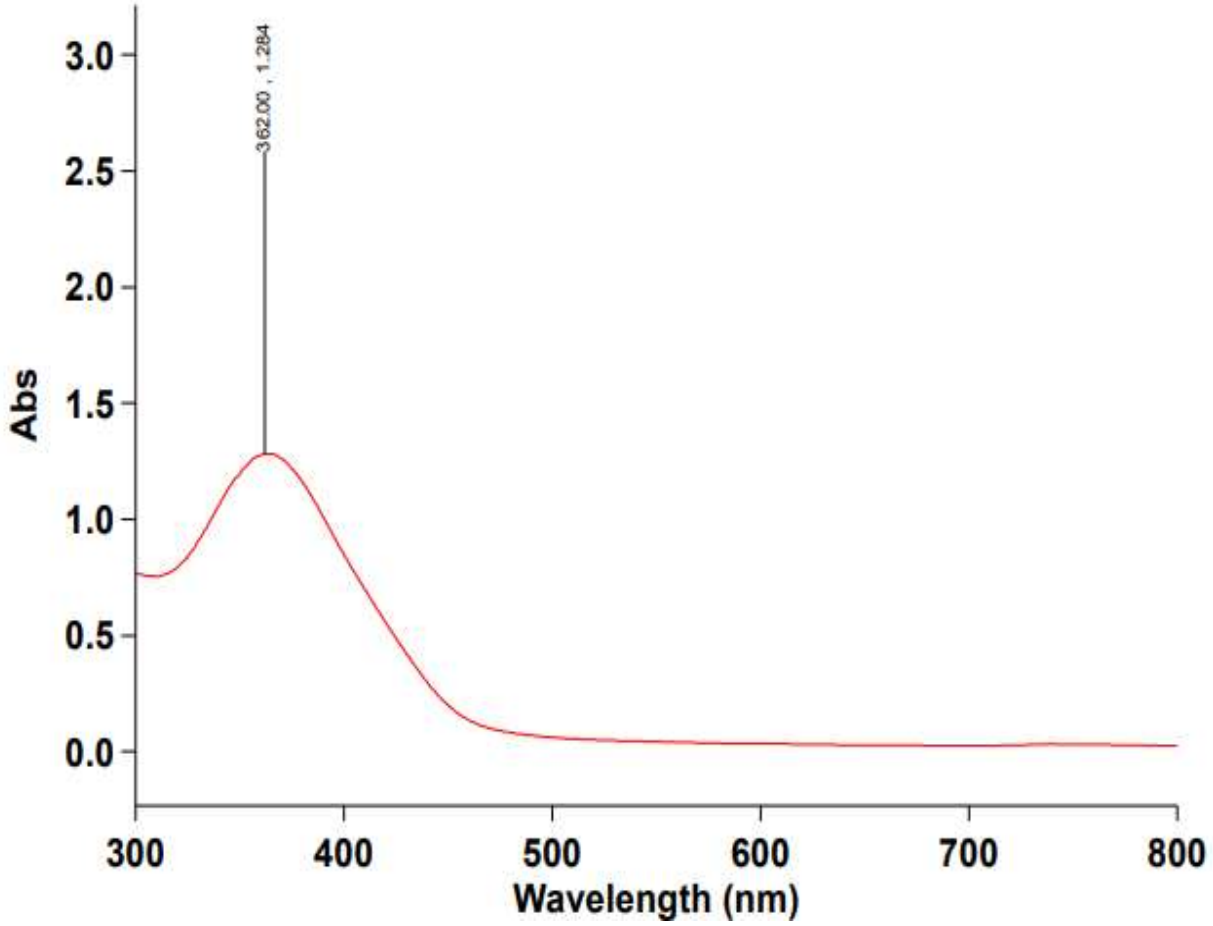

Figure 19: Ultraviolet–Visible Light Absorption Spectroscopy of PA2b

PA2b showed a UV peak of 362 nm wavelength

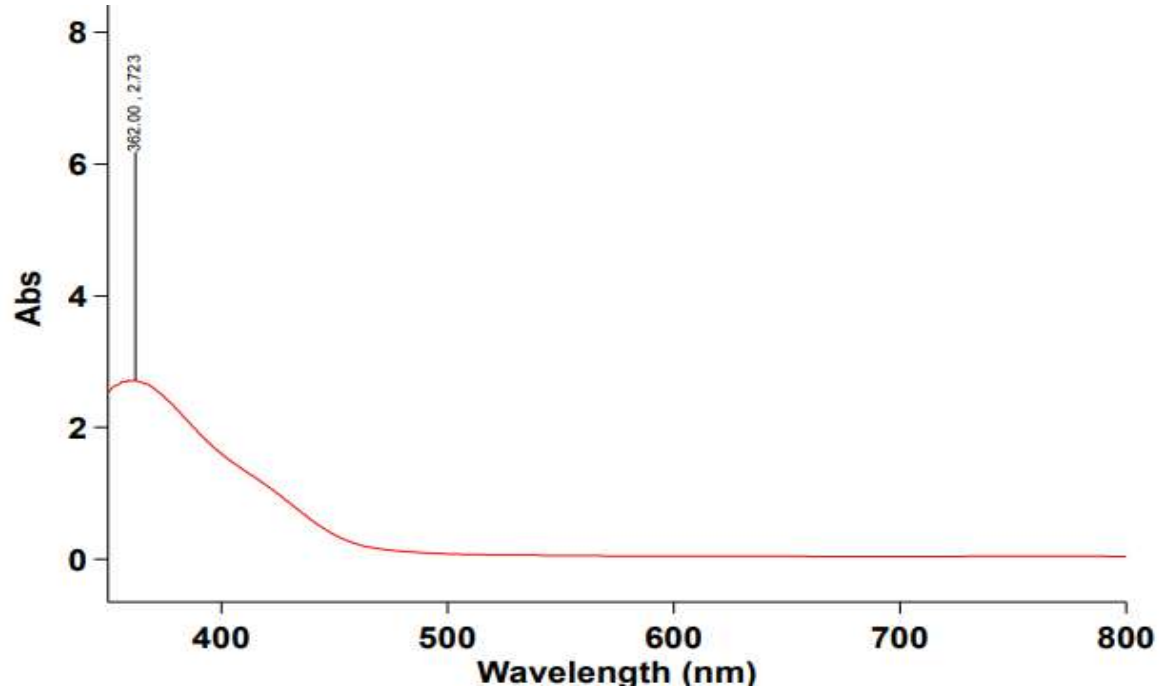

Figure 20: Ultraviolet–Visible Light Absorption Spectroscopy of PA3a

PA3a showed a UV peak of 362 nm wavelength

Ultraviolet–Visible Light Absorption Spectroscopy of Amoxicillin Pure Sample

Figure 21 illustrates the Ultraviolet–Visible Light Absorption Spectroscopy of amoxicillin pure sample.

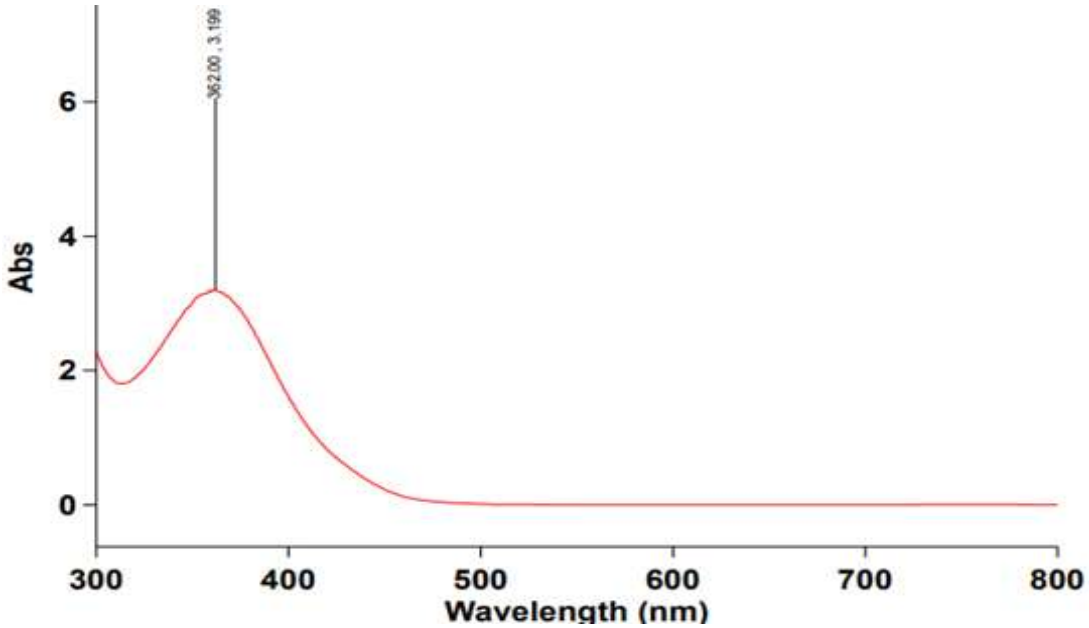

Figure 21: Ultraviolet – Visible Light Absorption Spectroscopy of Amoxicillin Pure Sample

Amoxicillin pure sample showed a UV peak of 362 nm wavelength.

Ultraviolet–Visible Light Absorption Spectroscopy of *Musa acuminata*-Based Amoxicillin Nanoparticles

Figures 22-25 illustrate the Ultraviolet–Visible Light Absorption Spectroscopy of *Musa acuminata*-based amoxicillin and metronidazole nanoparticles**.**

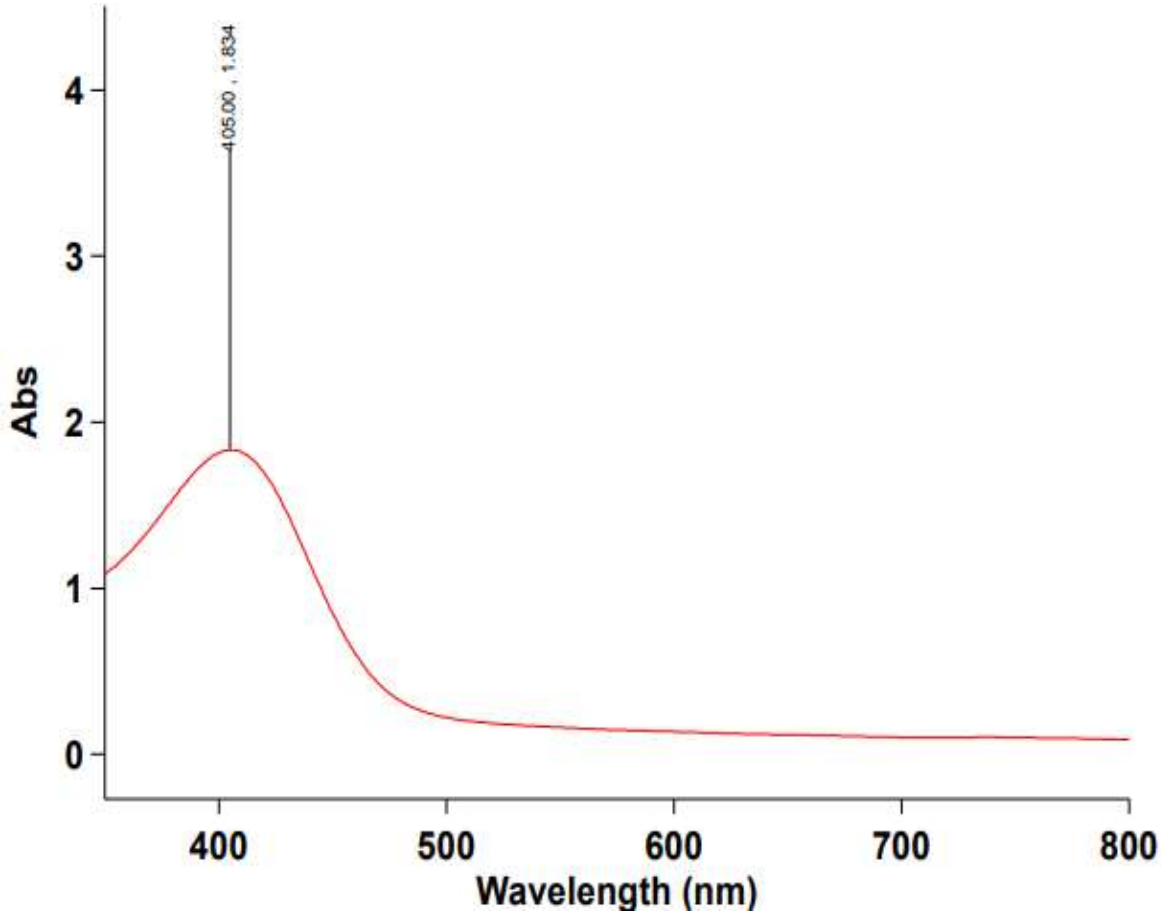

Figure 22: Ultraviolet–Visible Light Absorption Spectroscopy of BA1b

BA1b showed a UV peak of 405 nm wavelength.

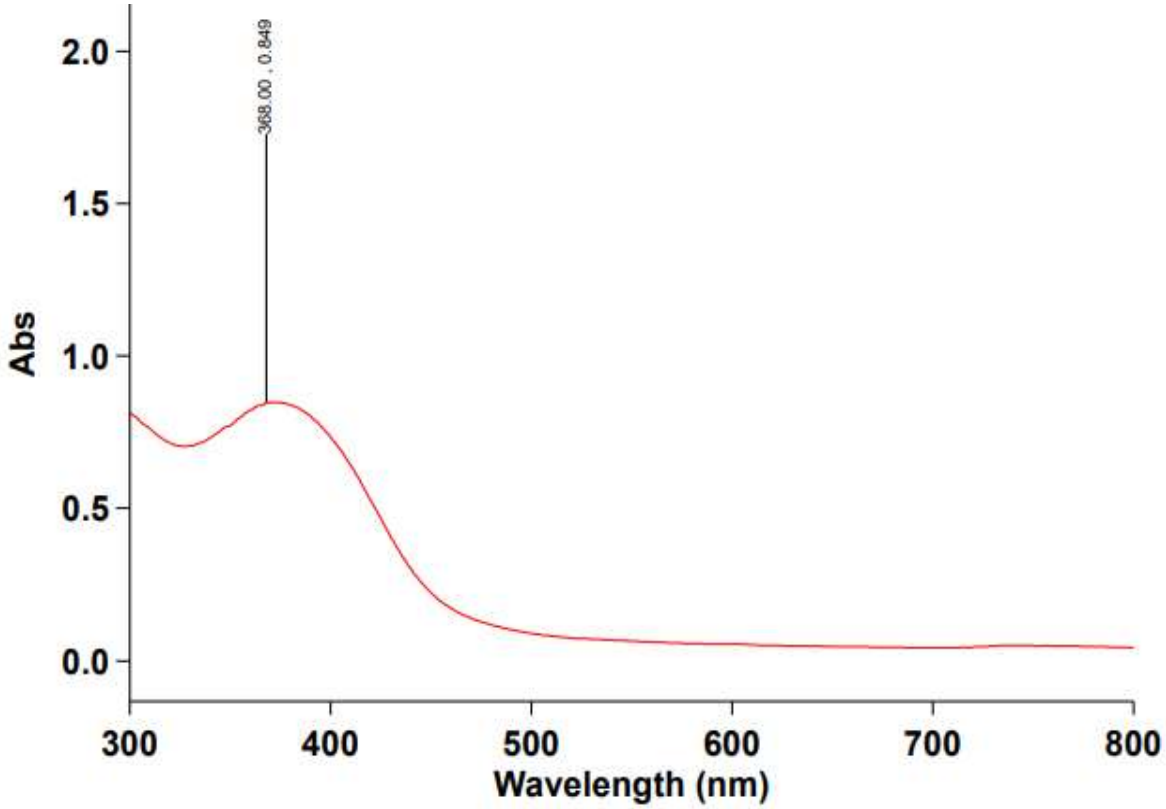

Figure 23: Ultraviolet–Visible Light Absorption Spectroscopy of BA2a

BA2a showed a UV peak of 368 nm wavelength.

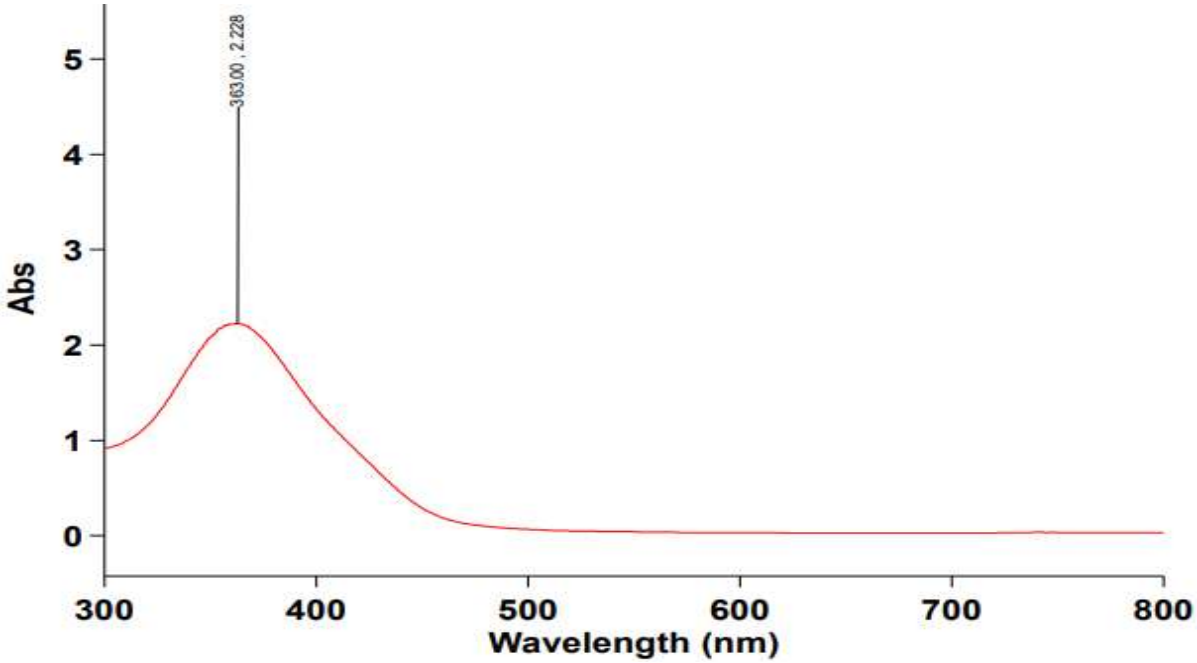

Figure 24: Ultraviolet–Visible Light Absorption Spectroscopy of BA3a

BA3a showed a UV peak of 363 nm wavelength.

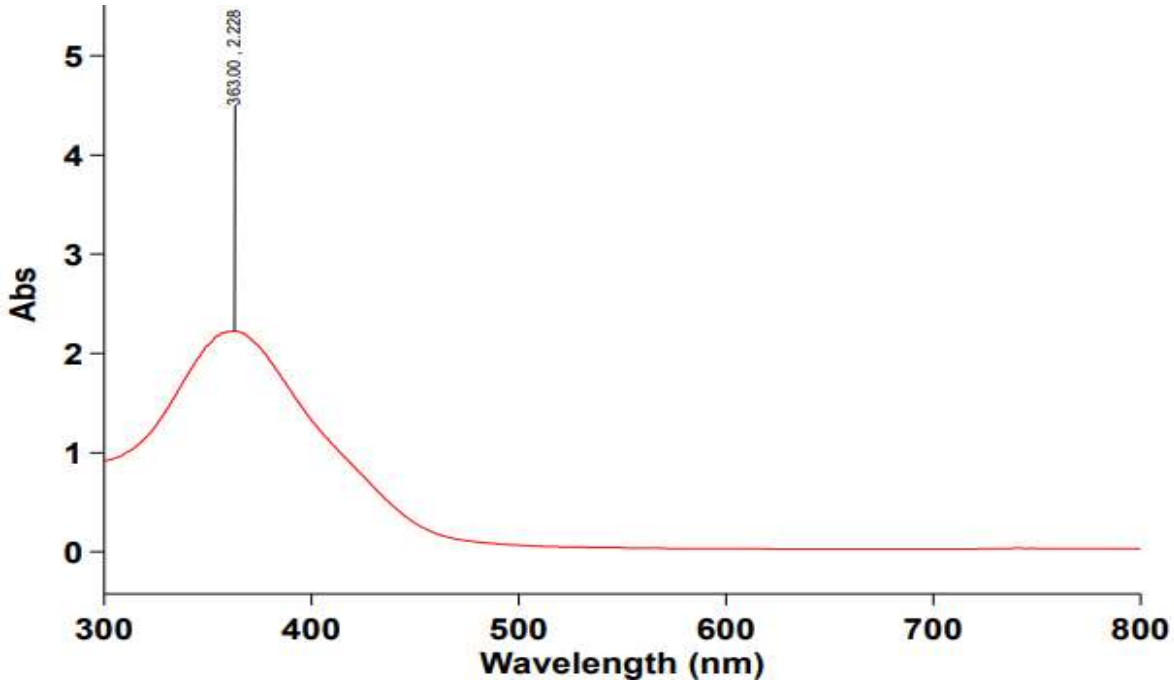

Figure 25: Ultraviolet–Visible Light Absorption Spectroscopy of BA3b

BA3b showed a UV peak of 363 nm wavelength.

Figure 21 showed UV-Visible spectra of amoxicillin pure sample, at absorption band of 362.3 nm and 263 nm respectively. While figures 22–25 showed absorption UV-Visible spectra band of Amoxicillin-loaded Musa acuminata-based nanoparticles at around 363–405 nm, where the absorbance upper limit of 405 nm was reported to be a typical plasmon band, which was as a result of the formation of silver nanoparticles. In addition, the center of absorption band was an operating factor which was the nucleation controller and also possess a stabilizing property.[22]

Conclusion

The results obtained from the formulation and evaluation of amoxicillin-loaded fruit-based nanoformulations clearly demonstrate the successful development of a stable and structurally modified nanodrug system using aqueous extracts of *Musa acuminata* (banana) and *Carica papaya* (pawpaw) for green synthesis of silver nanoparticles. Scanning Electron Microscopy (SEM) analysis confirmed the transformation of crystalline amoxicillin particles into predominantly spherical colloidal nanostructures with observable surface roughness. The increased surface irregularities and nanoscale size distribution indicate a significant enhancement in surface area, which is directly associated with improved dissolution behaviour and increased interaction potential with biological membranes. In contrast, the pure amoxicillin sample displayed larger, irregular crystalline morphology, confirming that nanoformulation altered its physical characteristics. Differential Scanning Calorimetry (DSC) studies revealed slight shifts in melting endotherms (92–94 °C) compared to pure amoxicillin (92 °C), indicating successful drug incorporation without significant chemical degradation. The absence of new sharp peaks suggests compatibility between amoxicillin and the fruit-mediated silver nanocarrier system. Fourier Transform Infrared Spectroscopy (FTIR) further confirmed drug nanoparticle interaction through characteristic peak shifts in hydroxyl and carbonyl functional groups, demonstrating

stabilization of the drug within the nanoparticle matrix. Ultraviolet–Visible spectroscopy showed surface plasmon resonance bands between 363–405 nm, confirming successful formation of silver nanoparticles and effective drug loading. Collectively, the findings establish that fruit-based green synthesized nanoparticles significantly modified the physicochemical properties of amoxicillin, enhanced its structural stability, and created a nanoplatform capable of improving dissolution characteristics and therapeutic performance. The study validates fruit-mediated nanotechnology as a sustainable, cost-effective, and pharmaceutically viable approach for advanced antibiotic delivery systems.

REFERENCES

1. Elzatahry AA, Eldin MM. (2008). Preparation and characterization of metronidazole-loaded chitosan nanoparticles for drug delivery application. Polymers Adv Technol. 19(12):1787-1791.
2. Ovenseri AC, Halilu EM. (2022). Formulation and in vitro evaluation of polymeric metronidazole nanoparticles. Pak J Pharm Sci. 35(5).
3. Steckiewicz KP, Cieciórski P, Barcińska E, et al. (2022). Silver nanoparticles as chlorhexidine and metronidazole drug delivery platforms: Their potential use in treating periodontitis. Int J Nanomedicine. 17:495-517.
4. Arias JL, Martínez-Soler GI, López-Viota M, Ruiz MA. (2010). Formulation of chitosan nanoparticles loaded with metronidazole for the treatment of infectious diseases. Lett Drug Des Discov. 7(2):70-78.
5. Cadinoiu AN, Rata DM, Daraba OM, et al. (2025). Metronidazole-loaded chitosan nanoparticles with antimicrobial activity against Clostridium perfringens. Pharmaceutics. 17(3):294.
6. Hano C, Abbasi BH. (2021). Plant-based green synthesis of nanoparticles: Production, characterization and applications. Biomolecules. 12(1):31.
7. Bawazeer S, Khan I, Rauf A, et al. (2022). Black pepper (Piper nigrum) fruit-based gold nanoparticles (BP-AuNPs): Synthesis, characterization, biological activities, and catalytic applications—A green approach. Green Process Synth. 11(1):11-28.
8. Hossain A, Abdallah Y, Ali MA, et al. (2019). Lemon-fruit-based green synthesis of zinc oxide nanoparticles and titanium dioxide nanoparticles against soft rot bacterial pathogen Dickeya dadantii. Biomolecules. 9(12):863.
9. Haq SI, Nisar M, Zahoor M, et al. (2023). Green fabrication of silver nanoparticles using Melia azedarach ripened fruit extract, their characterization, and biological properties. Green Process Synth. 12(1):20230029.
10. Jahura FT, Ferdousi FK, Kamal AHM, et al. (2025). Electrostatic adsorptive loading of ciprofloxacin and metronidazole on chitosan nanoparticles to prolong the drug delivery process with preserved antibacterial activities: Formulation and characterization. Nanoscale Adv. 2025;7(2):621-633.
11. Kameswaran S, Ramesh B, Gopal NO, Reddy AS. (2025). Plant-based nanoparticle synthesis. In: Plant-Based Nanoparticle Synthesis for Sustainable Agriculture. 20-29.
12. Khan AU, Malik N, Singh B, et al. (2023). Biosynthesis, and characterization of Zinc oxide nanoparticles (ZnONPs) obtained from the extract of waste of strawberry. J Umm Al-Qura Univ Appl Sci. 9(3):268-275.
13. Pathak K, Akhtar N. (2018). Nanoprobiotics: Current trends and future prospects. In: Nanotechnology in Nutraceuticals. 123-145.
14. Jackson, T. C., Agboke, A, A., Udofa, E. J., Ucheokoro, A. S., Udo, B. E. and Ifekpolugo, N. L. (2019). Characterization and release kinetics of metronidazole loaded silver nanoparticles prepared from Carica papaya leaf extract. Advances in Nanoparticles 8 (3): 47-54.

15. Chittaranjan Kole, Phullara Kole and Richard K. Marcus (2013). Nanobiotechnology can boost crop production and quality: first evidence from increased plant biomass, fruit yield and phytomedicine content in bitter melon (Momordica charantia). Journal of BioMedical Central Biotechnology, 46 (2): 519-528.

16. Silva, V. P., Alves, C. R., Dutra, R. F., Oliveira, J. E., Rondina, D. and Furtado, R. F. (2011). Biossensor amperométrico para determinação de peróxido de hidrogênio em leite. Eclética Química. Eclética Química, 36 (2):143-157.

17. Honary, S., Ghajar K., Khazaeli P. and Shalchian P. (2011). Preparation, Characterization and Antibacterial Properties of Silver-Chitosan Nanocomposites Using Different Molecular Weight Grades of Chitosan. Nanoparticles characterization, 10 (1): 71.

18. Belaabed, B., Lamouri, S., Naar, N., Bourson, P. and Hamady, S. O. S. (2010). Polyaniline-doped benzene sulfonic acid/epoxy resin composites: structural, morphological, thermal and dielectric behaviors. Polymer Journal, 42: 546-554.

19. Khan, M. A. M., Kumar, S., Ahamed, M., Alrokayan, S. A. and AlSalhi, M. S. (2011). Structural and thermal studies of silver nanoparticles and electrical transport study of their thin films. Nanoscale Research Letters, 6: 434.

20. Ajitha, B., Ashok, Kumar, Reddy, Y., Shamcer, S., Rajesh, K. M., Suneetha, Y. and Sreedhara, Reddy P. (2015). Lantana camara leaf extract mediated silver nanoparticles: Antibacterial, green catalyst. Journal of Photochemical and Photobiology B: Biology, 149: 84 – 92.

21. Suarez-Cerda, J., Alonso-Nunez, G., Espinoza-Gomez, H. and Flores-Lopez, I. Z. (2015). Synthesis, kinetics and photocatalytic study of ultra-small Ag-Nps obtained by a green chemistry method using an extact of Rosa Andeli double delight petals. The Journal of Colloid Interface Science, 458: 169-77.

22. Huang, H., Yuan, Q. and Yang, X. (2004). Preparation and characterization of metal-chitosan nanocomposites. Colloid Surface B, 39: 31-37.